Published in final edited form as:

J Am Chem Soc. 2017 March 01; 139(8): 3186–3195. doi:10.1021/jacs.6b12990.

Substrate and Lewis Acid Coordination Promote O–O Bond Cleavage of an Unreactive $L_2Cu^{II}_2(O_2^{2-})$ Species to Form $L_2Cu^{III}_2(O)_2$ Cores with Enhanced Oxidative Reactivity

Isaac Garcia-Bosch[*,†], **Ryan E. Cowley**[‡], **Daniel E. Díaz**[§], **Ryan L. Peterson**[§], **Edward I. Solomon**[*,‡], and **Kenneth D. Karlin**[*,§]

[†]Department of Chemistry, Southern Methodist University, Dallas, Texas 75275, United States

[‡]Department of Chemistry, Stanford University, Stanford, California 94305, United States

[§]Johns Hopkins University, Baltimore, Maryland 21218, United States

Abstract

Copper-dependent metalloenzymes are widespread throughout metabolic pathways, coupling the reduction of O_2 with the oxidation of organic substrates. Small-molecule synthetic analogs are useful platforms to generate L/Cu/O_2 species that reproduce the structural, spectroscopic, and reactive properties of some copper-/O_2-dependent enzymes. Landmark studies have shown that the conversion between dicopper(II)-peroxo species ($L_2Cu^{II}_2(O_2^{2-})$ either side-on peroxo, ^{S}**P**, or end-on *trans*-peroxo, ^{T}**P**) and dicopper(III)-bis(μ-oxo) ($L_2Cu^{III}_2(O^{2-})_2$:**O**) can be controlled through ligand design, reaction conditions (temperature, solvent, and counteranion), or substrate coordination. We recently published (*J. Am. Chem. Soc.* **2012**, *134*, 8513, DOI: 10.1021/ja300674m) the crystal structure of an unusual ^{S}**P** species $[(MeAN)_2Cu^{II}_2(O_2^{2-})]^{2+}$ (^{S}**P**^{MeAN}, MeAN: *N*-methyl-*N*,*N*-bis[3-(dimethylamino)propyl]amine) that featured an elongated O–O bond but did not lead to O–O cleavage or reactivity toward external substrates. Herein, we report that ^{S}**P**^{MeAN} can be activated to generate **O**^{MeAN} and perform the oxidation of external substrates by two complementary strategies: (i) coordination of substituted sodium phenolates to form the substrate-bound **O**^{MeAN}-**RPhO**$^{-}$ species that leads to *ortho*-hydroxylation in a tyrosinase-like fashion and (ii) addition of stoichiometric amounts (1 or 2 equiv) of Lewis acids (LA's) to form an unprecedented series of **O**-type species (**O**^{MeAN}-**LA**) able to oxidize C–H and O–H bonds. Spectroscopic, computational, and mechanistic studies emphasize the unique plasticity of the ^{S}**P**^{MeAN} core, which combines the assembly of exogenous reagents in the primary (phenolates) and secondary (Lewis acids association to the MeAN ligand) coordination spheres with O–O cleavage. These findings are reminiscent of the strategy followed by several metalloproteins and

[*]Corresponding Authors: igarciabosch@smu.edu, edward.solomon@stanford.edu, karlin@jhu.edu.

ORCID

Kenneth D. Karlin: 0000-0002-5675-7040

Notes

The authors declare no competing financial interest.

Supporting Information

The Supporting Information is available free of charge on the ACS Publications website at DOI: 10.1021/jacs.6b12990.

UV–vis experimental details and spectra, product analyses, rR experiments, DFT calculations, and xyz coordinates for the DFT structures (PDF)

highlight the possible implication of **O**-type species in copper-/dioxygen-dependent enzymes such as tyrosinase (Ty) and particulate methane monooxygenase (pMMO).

Graphical Abstract

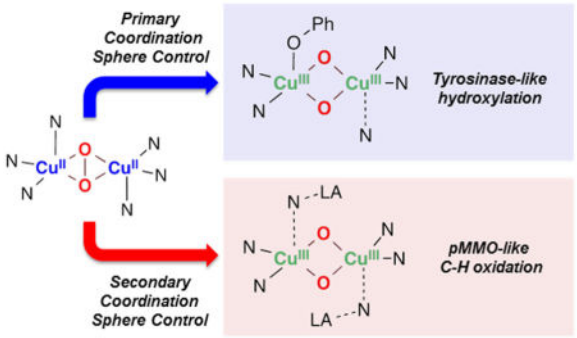

INTRODUCTION

Dicopper centers are a common motif found in the active sites of several O_2-activating metalloproteins that perform an array of physiological functions.[1] Tyrosinase (Ty) is a paradigmatic example of a metalloenzyme with a coupled dicopper active center (Figure 1A, left), which combines the reduction of dioxygen with the *ortho*-hydroxylation of tyrosine for melanin biosynthesis. Although its catalytic activity has been widely studied during the last several decades, there is still some debate on the identity of the reactive Cu_2/O_2 intermediate that is responsible for substrate oxidation. There is agreement on the first reaction step: Reduced Ty (dicopper(I)) reacts with dioxygen to form a dicopper(II) species with a side-on peroxide moiety (**^{S}P**). It is proposed that coordination of tyrosinate (phenolate form, Figure 1A center) to one of the copper(II) centers in oxy-Ty is followed by electrophilic attack of the peroxide to the aromatic ring.[1–3] Alternatively, some authors propose that prior to the electrophilic attack O–O cleavage occurs thus generating a dicopper(III) bis(μ-oxo) species (**O**) as the active oxidant (Figure 1A, right).[4,5]

Another ambiguity exists in copper-dependent particulate methane monooxygenase (pMMO). Detailed structural and spectroscopic studies have led to the proposal that the active site is a dicopper center with only two residues coordinating each Cu, with one Cu intriguingly bound to a N-terminal histidine (Figure 1B, left). Due to the technological implications of methane oxidation,[6,7] elucidation of the identity of the Cu/O_2 active species is of considerable general interest. However, the little information available has led to speculation that oxidation could be carried out by a $Cu^{II}(O_2^{2-})Cu^{II}$ (**^{S}P**), a $Cu^{III}(O^{2-})_2Cu^{III}$ (**O**), or a mixed-valent $Cu^{II}(O^{2-})_2Cu^{III}$ (and possibly protonated) species (Figure 1B, right).[5,8–11]

Several research groups, including ours, have extensively explored the O_2 chemistry of Cu(I) model complexes, which has led to the characterization of many distinct types of mononuclear and dinuclear Cu_n/O_2 species (Figure 2, top).[12–16] Especially relevant has been the study of the equilibrium between peroxodicopper(II) (**^{S}P** or **^{T}P**) and bis(μ-oxo)

dicopper(III) (**O**) species, which can be controlled by ligand design (including ligand donation to Cu), varying reaction conditions (i.e., temperature, solvent, and/or counter-anion), and substrate coordination (Figure 2, bottom).[12–21] From these studies, several general trends have emerged for controlling this equilibrium. It has been generally established that (i) tridentate ligation (i.e., N_3) favors ^{S}**P** formation while use of bidentate ligands (i.e., N_2) usually leads to **O** species; (ii) weakly coordinating counteranions and polar solvents favor **O** assemblies; and (iii) coordination of anionic substrates such as phenolates can lead to O–O cleavage prior to substrate oxidation.[4]

Recently, we published the crystal structure of the ^{S}**P** system $[(MeAN)_2Cu^{II}_2(O_2^{2-})]^{2+}$ (^{S}**P**^{MeAN}) (MeAN: *N*-methyl-*N*,*N*-bis[3-(dimethylamino)propyl]amine, Figure 3 top).[22] Strikingly, despite the unusually long O–O distance (1.54 Å) in this complex, there was no observable ^{S}**PMeAN/O**^{MeAN} equilibrium or reactivity with external substrates. We had attributed this to the weak backbonding from the Cu $3d_{xy}$ orbital to the peroxide σ^* orbital (Figure 3, middle), which is crucial for O–O cleavage.

Herein, we report that the oxidative properties of ^{S}**P**^{MeAN} can be activated by two different approaches (Figure 3, bottom). As previously reported in other systems, coordination of a series of substituted sodium phenolates leads to O–O cleavage to generate observable **O**^{MeAN}**-RPhO**$^{-}$ species that decay to generate the *ortho*-hydroxylated product.[4,23] A surprising and very new finding is that the ^{S}**PMeAN/O**^{MeAN} equilibrium can also be controlled by addition of various Lewis acids (**LA**) which are able to trigger the O–O cleavage of ^{S}**P**^{MeAN} species to generate distinctive **O**^{MeAN}**-LA** species with enhanced and tunable oxidative reactivity toward C–H and O–H bonds.

EXPERIMENTAL SECTION

General Considerations

All reagents and solvents were of commercially available quality except as noted. Acetone was distilled from Drierite under argon atmosphere. $[(MeAN)Cu^{I}](BAr^{F})$ (BAr^{F}: $B(C_6F_5)_4^{-}$) was synthesized as previously described.[24] Sodium phenolates were obtained using a synthetic method similar to previous results.[23] All UV–vis measurements were carried out using a Hewlett-Packard 8453 diode array spectrophotometer with a 10 mm quartz cell. The spectrometer was equipped with HP Chemstation software and a Unisoku cryostat for low temperature experiments. ^{1}H NMR spectra were recorded on a Bruker 400 instrument. Resonance Raman (rR) samples were excited using a Coherent I90C–K Kr^+ ion laser at 413.1 or 568.2 nm while the sample was immersed in a liquid-nitrogen-cooled (77 K) EPR finger dewar (Wilmad). Power was ~20 mW at the sample for the 413.1 nm line and ~130 mW at 568.2 nm. Data were recorded while rotating the sample to minimize photodecomposition. The spectra were recorded using a Spex 1877 CP triple monochromator with 600, 1200, or 2400 grooves/mm holographic spectrograph grating and detected by an Andor Newton CCD cooled to −80 °C (413.1 nm) or an Andor IDus CCD cooled to −80 °C (568.2 nm). Spectra were calibrated on the energy axis to toluene at room temperature.

$[(MeAN)_2Cu^{II}_2(O_2^{2-})]^{2+}$ ($^{S}P^{MeAN}$) Generation and Reaction with Sodium Phenolates

A 3 mL aliquot of a $[(MeAN)Cu^{I}](BAr^{F})$ solution (0.2 mM) in acetone was placed in a 10 mm path quartz cell equipped with a stir bar and capped with a rubber septum. After cooling down the cell to −90 °C (acetone), dioxygen was added to generate $[(MeAN)_2Cu^{II}_2(O_2^{2-})]^{2+}$ ($^{S}\mathbf{P}^{MeAN}$) (λ_{max}: 365 nm ε = 22 mM^{-1} cm^{-1}). After complete formation, 100 μL of an acetone solution containing excess of the corresponding substrate (substituted phenols, PPh_3, DHA, thioanisole, Me_2Fc, or Fc) was added. No spectral change was observed within 60 min after substrate addition. In contrast, addition of 100 μL of an acetone solution containing the corresponding 4-substituted sodium phenolate (to give a final concentration of 0.2 mM) to $^{S}\mathbf{P}^{MeAN}$ led to the immediate formation of the putative $[(MeAN)_2Cu^{III}_2(O^{2-})_2(R\text{-}PhO^{-})]^{+}$, followed by its decay (see Supporting Information). Kinetic analysis was performed by fitting the exponential decay of $[(MeAN)_2Cu^{III}_2(O^{2-})_2(R\text{-}PhO^{-})]^{+}$ at 400 nm. The k_{obs} obtained are summarized in the Supporting Information. Quantification of the corresponding catechols was performed using a method previously described (see Supporting Information).[25,26]

O^{MeAN}-LA Generation

A 0.2 mM solution of $^{S}\mathbf{P}^{MeAN}$ in acetone was prepared as described above at −90 °C. Then, 100 μL of an acetone solution containing the corresponding equivalents of Lewis acid (0.2 mM DMF·CF_3SO_3H, 0.1 mM $Sc(CF_3SO_3)_3$, or 0.1 mM $B(C_6F_5)_3$) was added to generate the corresponding $\mathbf{O}^{MeAN}$**-LA** species. See Supporting Information for titration experiments.

$^{S}P^{MeAN}/O^{MeAN}$-LA Reversibility

Formation of $\mathbf{O}^{MeAN}\mathbf{\text{-}2H^{+}}$ could be reversed by addition of proton sponge (1,8-bis(dimethylamino)-naphthalene) in excess (0.6 mM) leading to full regeneration of $^{S}\mathbf{P}^{MeAN}$ (see Supporting Information). $\mathbf{O}^{MeAN}\mathbf{\text{-}2H^{+}}$ could be formed again by readdition of DMF·CF_3SO_3H (0.6 mM was required for full formation, due to the presence of proton sponge excess in solution). Similarly, formation of $\mathbf{O}^{MeAN}\mathbf{\text{-}Sc^{3+}}$ could be reversed by addition of 1,10-phenanthroline in excess (0.8 mM), leading only to partial formation (75%) of $^{S}\mathbf{P}^{MeAN}$ (see Supporting Information) due to the ability of 1,10-phenanthroline to trap Cu(I) (430 and 455 nm bands, see Figure S9). $\mathbf{O}^{MeAN}\mathbf{\text{-}Sc^{3+}}$ could be partially formed again by readdition of $Sc(CF_3SO_3)_3$ (0.2 mM was required for full formation, due to the presence of excess 1,10-phenanthroline in solution). We could also reverse the formation of $\mathbf{O}^{MeAN}\mathbf{\text{-}2BR_3}$ by addition of TASF (tris(dimethylamino)sulfonium difluorotrimethylsilicate, a F^{-} source) in excess (0.6 mM), leading to partial formation (60%) of $^{S}\mathbf{P}^{MeAN}$ (see Supporting Information). $\mathbf{O}^{MeAN}\mathbf{\text{-}2BR_3}$ could be partially formed again by readdition of $B(C_6F_5)_3$.

O^{MeAN}-LA Reactivity toward Weak C–H Bonds and Substituted Phenols

After generation of the corresponding $\mathbf{O}^{MeAN}$**-LA** as described above, 100 μL of an acetone solution containing various amounts of the corresponding substrate (weak C–H bonds or substituted phenols) was added, causing the decay of the $\mathbf{O}^{MeAN}$**-LA** spectral features. The absorbance changes (λ = 410 nm) were fitted to single exponential decays. In all cases, a

linear correlation between the reaction rate (k_{obs}) and the substrate concentration was found, from which the second-order rate constants were obtained. Quantification of the oxidation products derived from the C–H (BNAH) and O–H oxidation (2,4-^{t}Bu-PhOH) was performed using methods previously described (see Supporting Information for details).[27]

Resonance Raman Experiments

In a typical experiment, 0.57 mL of a $[(MeAN)Cu^{I}]^{+}$ (1.0 mM) solution in acetone were placed in a 5 mm NMR tube capped with a septum. After cooling the tube to −90 °C (acetone/$N_{2(liq)}$ bath), dioxygen was bubbled through the solution mixture to generate $[(MeAN)_2Cu_2(O_2^{2-})]^{2+}$ (**^{S}P^{MeAN}**). To generate the $[(MeAN)_2Cu^{III}_2(O^{2-})_2(2,6\text{-}F_2\text{–}PhO^{-})]^{+}$, 50 μL of an acetone solution containing sodium 2,6-F_2-phenolate (3 mM) was added. To generate **O^{MeAN}-2H^{+}**, 50 μL of an acetone solution containing 2 equiv of DMF·CF_3SO_3H (1 mM) was added. To generate the **O^{MeAN}-Sc^{3+}**, 50μL of an acetone solution containing 1 equiv of $Sc(CF_3SO_3)_3$ (0.5 mM) was added. To generate the **O^{MeAN}-2BR$_3$**, 50 μL of an acetone solution containing 2 equiv of $B(C_6F_5)_3$ (0.5 mM) was added. Samples were frozen either 10 or 300 s after phenolate addition.

DFT Calculations

All calculations were performed with Gaussian 09 (revision D.01)[28] using the spin-unrestricted hybrid density functional B3LYP[29–31] and a split basis set (6-311G(d) on Cu, N, and O; 6-31G on all other atoms) on an ultrafine integration grid. All calculations included solvation correction (PCM, acetone solvent). Analytical frequencies were calculated on all geometry-optimized species to verify that the species were true local minima without negative frequencies. Calculations involving 2,6-difluorophenolate included Grimme's D3 dispersion correction.[32] For broken-symmetry singlet states of the side-on peroxos, the Yamaguchi formalism[33] was used to eliminate triplet contamination and obtain a corrected SCF energy (eq 1, where ^1E is the corrected singlet energy, ^{BS}E and ^3E are energies of the broken-symmetry and triplet states, respectively, and $\langle S^2\rangle_{BS}$ is the calculated spin expectation value obtained from the broken-symmetry wave function).

$$^1E = \frac{2^{BS}E - (\langle S^2\rangle_{BS} \cdot {}^3E)}{2 - \langle S^2\rangle_{BS}} \quad (1)$$

For time-dependent DFT calculations, the calculated electronic absorption spectra were generated using SWizard[34] with 3000 cm^{-1} line widths and Gaussian bandshapes.

RESULTS AND DISCUSSION

Ortho Hydroxylation of Phenolates

We previously reported[22] that **^{S}P^{MeAN}** was unreactive toward external substrates including 9,10-dihydroanthracene (DHA, $BDFE_{(C–H)}$ = 76 kcal/mol), 2,4-di-*tert*-butylphenol (2,4-DTB-PhOH, $BDFE_{(O–H)}$ = 82 kcal/mol), and thioanisole. We expanded the substrate scope to other substrates even more prone to oxidation by electrophilic metal-peroxo species

including 1-benzyl-1,4-dihydronicotinamide (BNAH, $BDFE_{(C–H)}$ = 71 kcal/mol),[27] 2,6-di-*tert*-butyl-4-methoxyphenol ($BDFE_{(O–H)}$ = 80 kcal/mol),[35] and triphenylphosphine, but no decay of the $^{S}\mathbf{P}^{MeAN}$ UV–vis features were observed, even 1 h after addition of the substrate. We speculated that the unreactive nature of $^{S}\mathbf{P}^{MeAN}$ was due to the inability of the complex to form an $\mathbf{O}^{MeAN}$ species, which typically oxidizes these types of substrates.[14,36]

This has led us to attempt oxidation of other types of substrates. $^{S}\mathbf{P}^{MeAN}$ reacts with a series of 4-substituted sodium phenolates (4-MeO, 4-Me, 4-H, 4-Cl, and 4-CN), which generates the corresponding *ortho*-hydroxylated products in a tyrosinase-like fashion in moderate yields (30–40%). Kinetic studies using the series of 4-R-PhO^- were conducted in order to gather mechanistic details for this oxidative process. Addition of the substrate to $^{S}\mathbf{P}^{MeAN}$ caused an immediate change of the UV–vis spectrum, followed by a fast first-order decay (see Supporting Information for details). The disappearance of these fleeting species was followed by UV–vis and fit to an exponential decay. When plotting the reaction rates obtained (k_{obs}) for the varying substrates against the Hammett parameter (σ^+), a linear correlation was found ($\rho = -2.2$), suggesting an electrophilic aromatic substitution mechanism (see Figure S2). These findings are analogous to the results found by Stack and co-workers and other research groups,[4,23] pointing toward a mechanism where substrate coordination to $^{S}\mathbf{P}^{MeAN}$ triggers O–O cleavage to form a $[(MeAN)_2Cu^{III}{}_2(O^{2-})_2(R\text{-}PhO^-)]^+$ ($\mathbf{O}^{MeAN}$-$\mathbf{RPhO}^-$) intermediate prior to substrate oxidation (Figure 4, top).

In a recent contribution, Serrano-Plana et al. reported that the MeAN-inspired $[(m\text{-}XYL^{MeAN})_2Cu^{III}{}_2(O^{2-})_2]^{2+}$ complex was also able to perform the *ortho*-hydroxylation/defluorination of 2-fluoro-substituted phenolates in a selective fashion.[26] Using similar reaction conditions, we found that the $^{S}\mathbf{P}^{MeAN}$ oxidized 2,6-F_2-phenolate to the corresponding 3-F-catechol in moderate yield (30%). Interestingly, coordination of the substrate to $^{S}\mathbf{P}^{MeAN}$ (Figure 4 bottom right, brown spectrum) was found to form a phenolate-bound **O**-type species $[(MeAN)_2Cu^{III}{}_2\text{-}(O^{2-})_2(F_2PhO^-)]^+$ ($\mathbf{O}^{MeAN}$-$\mathbf{F_2PhO}^-$, Figure 4, blue spectrum) with spectroscopic characteristics similar to other phenolate-coordinated **O** species.[23]

Due to the slower reaction rate found for the fluorinated substrate, we were able to cold-trap and characterize $\mathbf{O}^{MeAN}$-$\mathbf{F_2PhO}^-$ by rR spectroscopy (Figure 4, bottom right inset). Upon laser excitation at 568.2 nm, three main isotope-sensitive modes were observed at 663 ($\Delta(^{18}O_2) = -23\ cm^{-1}$), 604 ($\Delta(^{18}O_2) = -13\ cm^{-1}$), and 590 cm^{-1} ($\Delta(^{18}O_2) = -31\ cm^{-1}$), which are assigned as $\nu_{Cu–O}$ vibrations of the Cu_2O_2 core of $\mathbf{O}^{MeAN}$-$\mathbf{F_2PhO}^-$.[37] The characteristic $\nu_{O–O} = 722\ cm^{-1}$ mode of $^{S}\mathbf{P}^{MeAN}$ (Figure 4, bottom left inset) was not observed after phenolate addition, demonstrating full conversion to $\mathbf{O}^{MeAN}$-$\mathbf{F_2PhO}^-$. One additional mode with very small $^{16/18}O_2$ sensitivity (513 cm^{-1}, $\Delta(^{18}O_2) = -3\ cm^{-1}$) is also observed in $\mathbf{O}^{MeAN}$-$\mathbf{F_2PhO}^-$, which is likely a predominantly Cu–N or $Cu–O_{phenolate}$ mode that gains minor $^{16/18}O_2$ isotope sensitivity through mixing of a core Cu–O mode. The number of observed Cu–O modes in rR can be a useful reporter of the local symmetry of the Cu_2O_2 core, since only symmetric modes (i.e., with A symmetry) are rR active.[38] A maximally symmetric Cu_2O_2 bis(μ-oxo) of D_{2h} symmetry has only one of four Cu–O stretching modes symmetry allowed (A_1), while descent in symmetry to C_{2h} or C_{2v} results in two allowed modes (A_g), and further descent to C_s results in all four modes being symmetry

allowed (A'). The observation of three Cu–O modes in **O^{MeAN}-F$_2$PhO$^-$** thus suggests local pseudo-C_s symmetry, which is consistent with coordination of phenolate to one Cu.

DFT calculations were used to support the assignment of **O^{MeAN}-F$_2$PhO$^-$** and investigate the role of phenolate in modulating the **^{S}P/O** equilibrium. Two different isomers of the resulting **O^{MeAN}-F$_2$PhO$^-$** adduct were optimized (Figure 4, bottom left): one with the phenolate coordinated to one of the copper(III) centers in an axial position (**O^{MeAN}-F$_2$PhO$^-$ (ax)**), which was 10 kcal/mol higher in energy than the other with phenolate coordinated in an equatorial position (**O^{MeAN}-F$_2$PhO$^-$ (eq)**). Only the equatorial phenolate model correctly reproduced the observed direction of the **^{S}P/O** equilibrium, with the bis(μ-oxo) favored over the side-on peroxo isomer by 7.7 kcal/mol (for the axial phenolate, **^{S}P** was favored by 3.1 kcal/mol). Furthermore, calculated normal modes for **O^{MeAN}-F$_2$PhO$^-$ (eq)** better matched the experimental rR data than **O^{MeAN}-F$_2$PhO$^-$ (ax)** (See Supporting Information for details); thus, the observed species is most consistent with possessing a **O^{MeAN}-F$_2$PhO$^-$ (eq)** structure.

TD-DFT calculations of **O^{MeAN}-F$_2$PhO$^-$ (eq)** also reproduced the absorption spectrum of the observed bis(μ-oxo) species. While both **O^{MeAN}-F$_2$PhO$^-$** isomers showed typical spectra for a **O**-type species (two intense absorptions centered around 300 and 400 nm), only the spectrum calculated for the **O^{MeAN}-F$_2$PhO$^-$ (eq)** isomer had the intense lower energy bands (450–550 nm), which are assigned as phenolate-to-copper charge transfer transitions based on orbital analysis. This arises from the orientation of the phenolate in the Cu_2O_2 plane, which provides good overlap between the donor (phenolate π) and acceptor (Cu $d_{x^2-y^2}$) orbitals and thus intense LMCT character.

As previously reported by Stack and co-workers,[37] we propose that initial coordination of the phenolate occurs at one of the available axial positions (**O^{MeAN}-F$_2$PhO$^-$ (ax)**) and then rapidly isomerizes to the spectroscopically observed equatorial form (**O^{MeAN}-F$_2$PhO$^-$ (eq)**). The substrate is then electrophilically attacked by the $Cu^{III}_2(O^{2-})_2$ core. In the axial form, DFT calculations suggest there is a weak Cu^{III}···F interaction (d(Cu···F) = 3.02 Å) worth ~2 kcal/mol as compared to that of the phenolate-bound complex without the *ortho* F (calculated using 2,4-F_2-phenolate, see Supporting Information). However, this weak Cu–F interaction is not sufficiently strong to prevent isomerization to the equatorially bound species (**O^{MeAN}-F$_2$PhO$^-$ (eq)**, 10 kcal/mol more stable) which would then lead to *ortho*-hydroxylation and defluorination.

O–O Cleavage Promoted by Lewis Acids

Due to the unreactive character of **^{S}P^{MeAN}** core, we wondered if addition of Lewis acids could boost its oxidative power, as observed with iron or manganese oxo (or peroxo) complexes.[39–42] Strikingly, addition of $Sc(CF_3SO_3)_3$ to **^{S}P^{MeAN}** (λ_{max} = 365 nm; ε = 22 mM^{-1} cm^{-1}) led to the formation of a new species with UV–vis features (Figure 5) that are characteristic of **O**-type complexes (λ_{max} = 412 nm; ε = 24 mM^{-1} cm^{-1}). Titration experiments established that only 1 equiv of Sc^{3+} was required for full formation of the adduct, thus formulated as **O^{MeAN}-Sc^{3+}** (Figure 5, top). Surprisingly, this reactivity is not exclusive for Sc^{3+}: Addition of nonmetallic Lewis acids such as $B(C_6F_5)_3$ or

DMF·CF_3SO_3H (Brønsted acid) also led to O–O cleavage and formation of **O**-type species. In these latter cases, titration experiments suggested that 2 equiv of $B(C_6F_5)_3$ or 2 equiv of DMF·CF_3SO_3H were necessary to form the corresponding adducts, thus formulating the products as the species $\mathbf{O^{MeAN}\text{-}2BR_3}$ (λ_{max} = 414 nm; ε = 24 mM^{-1} cm^{-1}) and $\mathbf{O^{MeAN}\text{-}2H^+}$ (λ_{max} = 410 nm; ε = 21 mM^{-1} cm^{-1}), respectively.

We made use of rR spectroscopy to characterize this family of $\mathbf{O^{MeAN}\text{-}LA}$ species. Laser excitation ($\lambda_{exc.}$ = 413 nm) of samples of $\mathbf{O^{MeAN}\text{-}Sc^{3+}}$, $\mathbf{O^{MeAN}\text{-}2BR_3}$ and $\mathbf{O^{MeAN}\text{-}2H^+}$ prepared with $^{16}O_2$ and $^{18}O_2$ enhanced three isotope-sensitive modes at 514–602 cm^{-1} (ν_2, ν_3, and ν_4 in Figure 5 middle) characteristic of Cu–O core modes of **O**-type species, and similar to $\mathbf{O^{MeAN}\text{-}F_2PhO^-}$. Combination bands ($\nu_2$ + ν_4 at ~1120 cm^{-1} and ν_1 + ν_4 at ~740 cm^{-1}, where ν_1 is a low-energy isotope-insensitive mode at ~140 cm^{-1}) and an overtone ($2\nu_4$ at ~1210 cm^{-1}) are also observed.[43,44] Surprisingly, the rR spectra of the different $\mathbf{O^{MeAN}\text{-}LA}$ were almost superimposable, suggesting that the bis(μ-oxo) dicopper(III) cores had very similar structures. This indicates that the Lewis acids are not interacting directly with the oxygen atoms of the Cu_2O_2 core but rather coordinating to the axial N donors of the ligand. DFT calculations support this hypothesis: We found that in the computationally optimized structures for all three $\mathbf{O^{MeAN}\text{-}LA}$,[43,45] the Lewis acid was bound to the N ligands of MeAN (Figure 5, bottom). Moreover, our calculations were able to reproduce the stoichiometry found in our titration experiments: While the Sc^{3+} ion was able to coordinate one N from each of the MeAN ligands, two molecules of borane or acid were required for O–O cleavage. The stabilization energy calculated upon binding of the Lewis acid was found to be very similar for all three $\mathbf{O^{MeAN}\text{-}LA}$ complexes (between 3 and 6 kcal/mol, see Supporting Information). The optimized geometries for the $\mathbf{O^{MeAN}\text{-}LA}$ species are very similar in all the cases, where the copper(III) ions are bound to two of the N donors of the MeAN ligand and two oxygen atoms. Similarly, the calculated UV–vis and rR features were also nearly identical for all adducts, corroborating our experimental findings (see Supporting Information).

To investigate the role of Lewis acids in stabilizing the $\mathbf{O^{MeAN}}$ isomer relative to $\mathbf{{}^{S}P^{MeAN}}$, we optimized a structure of $\mathbf{{}^{S}P^{MeAN}}$ with both axial N ligand arms uncoordinated (Figure 6A, right). Although removing the axial ligands is calculated to cost ΔG = +8 kcal/mol, the "arm off" isomer favors an **O** configuration by ΔG = −3.5 kcal/mol, which is similar to the preference for **O** in the Lewis acid adducts (–3.5 to −6.7 kcal/mol stabilization of **O** relative to that of $\mathbf{{}^{S}P}$, Figure S23), and inverse from that of the "arm on" isomer, which favors the $\mathbf{{}^{S}P}$ configuration by ΔG = −2.2 kcal/mol. The "arm off" peroxo model featured a longer O–O bond (1.504 vs 1.488 Å) and shorter Cu–O (average 1.93 vs 1.98 Å) and Cu–N bonds (1.99 vs 2.03 Å) compared to the "arm on" structure (Figure 6A, top). The "arm off" structure thus allows better orbital overlap with the equatorial N ligands, which is also consistent with the less pyramidalized Cu (3° deviation from the Cu_2O_2 plane vs 27°, Figure 6A, center). Therefore, by sequestering the axial N, addition of Lewis acid allows stronger equatorial ligand donation, which in turn leads to a greater degree of O_2 activation (Figure S26) that results in formation of a low energy $\mathbf{O^{MeAN}}$ species via O–O cleavage.[43]

Surprisingly, the O–O bond cleavage could be reversed by addition of Lewis acid chelating reagents. For example, 1,10-phenanthroline was able to capture Sc^{3+} from $\mathbf{O^{MeAN}\text{-}Sc^{3+}}$ to

recover 75% of $^{S}\mathbf{P}^{\mathbf{MeAN}}$, and 1,8-bis(dimethylamino)-naphthalene (proton sponge) was added to $\mathbf{O}^{\mathbf{MeAN}}\mathbf{-2H}^{+}$ to fully regenerate $^{S}\mathbf{P}^{\mathbf{MeAN}}$ (see Supporting Information for details).[46] Recently, Que and co-workers have studied the effect of Sc^{3+} addition to the mononuclear nonheme iron(II) complex, which when combined with dioxygen led to the formation of a metastable iron(III)-peroxo-Sc^{3+} adduct that then irreversibly transformed to a corresponding high-valent iron(IV)-oxo complex (Figure 6, right).[47] Nam and co-workers expanded that reactivity to other Lewis acids, where depending on the nature of the Lewis acid identity, the iron(III)-peroxo-LA adduct could be reduced to liberate dioxygen (LA: Ca^{2+}, Sr^{2+}) or led to O–O cleavage (LA: Zn^{2+}, Lu^{3+}, Y^{3+}, Sc^{3+}).[48] To the best of our knowledge, the reactivity reported herein is the first example of Lewis acid mediated reversible O–O bond cleavage/formation, which is reminiscent of the chemistry occurring in water oxidation process catalyzed by the Mn_4Ca^{2+} cluster in photosystem II (Figure 6, left).

Reactivity of O^{MeAN}-LA toward C–H Bonds

At this point, we decided to test the reactivity of $\mathbf{O}^{\mathbf{MeAN}}\mathbf{-LA}$ species toward external substrates, alongside the analogous parent $^{S}\mathbf{P}^{\mathbf{MeAN}}$ complex. Surprisingly, we found that both $^{S}\mathbf{P}^{\mathbf{MeAN}}$ and $\mathbf{O}^{\mathbf{MeAN}}\mathbf{-LA}$ were unable to oxidize substrates that are prone to accept O atoms, such as triphenylphosphine and thioanisole.[14] The first difference in reactivity was found when substrate one-electron ($1e^{-}$) reductants were added. While both $^{S}\mathbf{P}^{\mathbf{MeAN}}$ and $\mathbf{O}^{\mathbf{MeAN}}\mathbf{-LA}$ reacted with strong $1e^{-}$ reducing reagents ($Me_{10}Fc$ or Me_8Fc, $E^0 < -0.4$ V vs $Fc^{+/0}$), only the $\mathbf{O}^{\mathbf{MeAN}}\mathbf{-LA}$ series was found to be able to oxidize the more difficult substrate, Me_2Fc ($E^0 = -0.12$ V vs $Fc^{+/0}$). Based on this bracketing analysis, we can conclude that the $\mathbf{O}^{\mathbf{MeAN}}\mathbf{-LA}$ species possess higher reduction potentials than $^{S}\mathbf{P}^{\mathbf{MeAN}}$, that is, they are stronger one-electron oxidants.

Another main difference in reactivity was found in reactions with substrates with weak C–H bonds. As previously reported, $^{S}\mathbf{P}^{\mathbf{MeAN}}$ was not able to oxidize dihydroanthracene (DHA; BDE: 78 kcal/mol).[22] Here, we find that the $\mathbf{O}^{\mathbf{MeAN}}\mathbf{-LA}$ species are also not able to abstract a H atom ($H^{\bullet}$) from DHA. However, when 1-benzyl-1,4-dihydronicotinamide (BNAH, BDE: 71 kcal/mol) was used, the $^{S}\mathbf{P}^{\mathbf{MeAN}}$ core was unreactive, but the series of $\mathbf{O}^{\mathbf{MeAN}}\mathbf{-LA}$ complexes reacted to generate the corresponding BNA^{+} product in 75–99% yield (Figure 7A, see Supporting Information for product quantification). Kinetic interrogation of this reaction showed pseudo-first-order decay behavior with respect to [BNAH] (see Supporting Information). Second-order rate constants were obtained (Table 1), with the $\mathbf{O}^{\mathbf{MeAN}}\mathbf{-2BR_3}$ reacting slightly faster than the $\mathbf{O}^{\mathbf{MeAN}}\mathbf{-2H}^{+}$ and $\mathbf{O}^{\mathbf{MeAN}}\mathbf{-Sc}^{\mathbf{3+}}$ cores (Table 1). The same set of experiments was carried out using the deuterated analogue BNAD, which led to the determination of primary kinetic isotope effects of 10.3 for $\mathbf{O}^{\mathbf{MeAN}}\mathbf{-2BR_3}$, 8.5 for $\mathbf{O}^{\mathbf{MeAN}}\mathbf{-2H}^{+}$, and 6.1 for $\mathbf{O}^{\mathbf{MeAN}}\mathbf{-Sc}^{\mathbf{3+}}$ (temperature: −90 °C). These values are consistent with C–H bond cleavage during the rate-determining step (r.d.s.).

Two mechanistic scenarios are possible: (i) stepwise $H^{\bullet}$ transfer (HAT) during the r.d.s. followed by e^{-} transfer or (ii) a one-step hydride (H^{-}) transfer during the r.d.s. We previously reported that a copper(I)-dioxygen adduct, formally a cupric-superoxide species, also preferentially effected the energetically more difficult $H^{\bullet}$-abstraction in preference to hydride abstraction chemistry.[27] In order to distinguish between these two possibilities, the

reaction between 1,3-dimethyl-2,3-dihydrobenzimidazole (BzImH) and the **O^{MeAN}-LA** series was tested. BzImH is a better hydride donor (49.5 kcal/mol heterolytic C–H BDE, vs 64.2 kcal/mol for BNAH) but a poorer H$^{\bullet}$ donor (73.4 kcal/mol homolytic C–H BDE vs 70.7 kcal/mol for BNAH). For all the **O^{MeAN}-LA** complexes, slower reaction rates for BzImH were observed (5–10 times slower, see Table 1), consistent with HAT during the r.d.s. (Figure 7) rather than concerted hydride transfer.

The reactivity described herein is consistent with previous reports that suggest that **O**-type species rather than **^{S}P** carry out the intra- or intermolecular oxidation of C–H bonds.[14,20,21] Although the difference in the reaction rates found for the different **O^{MeAN}-LA** species was modest (the **O^{MeAN}-2BR3** adduct was 2–3 times faster for all the substrates tested), it is worth mentioning that subtle changes in the stereoelectronic properties of the **O^{MeAN}-LA** cores, tuned by the use of different Lewis acids, could lead to differential and useful oxidation kinetics/chemistries. Our findings are in accordance with the data reported by Goldberg and co-workers, where the $Mn^{IV}(O)$:$B(C_6F_5)_3$ adduct ($[(TBP_8Cz^{\bullet+})Mn^{IV}(O):B(C_6F_5)_3]$) ($TBP_8Cz$ = octakis(*p-tert*-butylphenyl)corrolazinato) was found to perform the oxidation of C–H and O–H bonds via HAT faster than the corresponding $Mn^{IV}(O):Zn^{2+}$ adduct.[40,46]

Reactivity of O^{MeAN}-LA toward O–H Bonds

We have also explored the reactivity of the **^{S}P^{MeAN}** and **O^{MeAN}-LA** toward phenols. As previously reported, **^{S}P^{MeAN}** was found to be unreactive toward 2,4-$^{t}Bu_2$-phenol. As shown in Table 2, we tested the reactivity of **^{S}PMeAN/O^{MeAN}-LA** with a series of 4-substituted phenols with different O–H bond strengths and varying one-electron redox potentials (E^0). The **^{S}P^{MeAN}** complex was unreactive toward all of the phenols tested. However, the family of **O^{MeAN}-LA** cores was found to be reactive in the $1e^-/1H^+$ oxidation of phenols with BDEs lower than 84.6 kcal/mol and E^0 values lower than 1.12 V (Table 2, see Supporting Information for product quantification). The oxidation of 2,4-di-*tert*-butylphenol (2,4-^{t}Bu-PhOH) by the **O^{MeAN}-LA** cores led to the formation of the C–C coupling product (see Supporting Information for details on its detection and quantification).

Kinetic analyses of these reactions (Figure 8A) led to pseudo-first-order behavior with varying phenol concentrations and gave linear second-order plots allowing for the calculation of second-order rate constants, which are listed in Table 2. Overall, the trends found in phenol (O–H) oxidation are reversed from BNAH/BzImH (C–H) oxidation; the **O^{MeAN}-2H^{+}** and **O^{MeAN}-Sc^{3+}** complexes exhibit higher reaction rates (10–20 times) than the corresponding **O^{MeAN}-2BR$_3$** complex. When the reaction rates found were plotted against the $1e^-$reduction potentials of the phenols ($(RT/F)\cdot\ln(k)$ vs E^0), a linear correlation was obtained (Figure 8A, right).[35,49,50]

According to Marcus theory, the slope value obtained in this correlation can be used to distinguish between pure H$^{\bullet}$ transfer (HAT: slope = 0.0) from electron transfer (ET) or proton-coupled electron transfer (PCET: slope = −0.5 if $\Delta G^0_{et} < 0$; slope = −1.0 if $\Delta G^0_{et} > 0$).[49] The low KIE's observed (1.1–1.2, see Figure S18) along with the slope values (around −1.0) suggest a mechanistic scenario where endergonic electron transfer (ET) is followed by

fast proton transfer (PT). This proposal is in agreement with the $1e^-$ reactivity observed with substituted Fc (see Supporting Information), where the **O^{MeAN}-LA** complexes were only reduced by donors with E^0 equal or lower than −0.12 V (e.g., Me_2Fc), a value substantially lower (by 1.0–1.5 V) than the phenol $1e^-$ oxidation potential. (The **O^{MeAN}-LA** complexes were not reduced by Fc, E^0 = 0.0 V vs $Fc^{+/0}$.) An alternative mechanism with rate-limiting PT followed by $1e^-$ oxidation of the phenolate is not consistent with the large negative slope of the rate/potential correlation or the small primary H/D isotope effect.

The mechanistic study of the $1e^-/1H^+$ oxidation of phenols by LCu/O_2 derived species was first reported by Itoh and coworkers, where **^{S}P** and **O** species were found to oxidize 4-substituted phenols via proton-coupled electron transfer (PCET) with somewhat smaller slopes (−0.72 and −0.71, respectively) and similar KIEs (1.2–1.6 and 1.2–1.5, respectively), where the smaller slope indicates less endergonic ET such that ET and PT are kinetically similar.[49] Similarly, Costas and co-workers reported that end-on peroxo species are also able to oxidize phenols via PCET (slope = −0.49, KIE: 1.5–2.0), where the slope of ~ −0.5 is consistent with exergonic ET.[51] Very recently, we reported that a mononuclear end-on copper(II)-superoxide intermediate (**^{E}S**) oxidizes phenols via HAT (slope: −0.29, KIE: 9.0).[35] The results reported herein (stepwise ET-PT, slope = −1.0, KIE: 1.1–1.3) are unprecedented for the reactivity shown by Cu/O_2-derived species, in particular the ability to perform substrate oxidation that involves endergonic ET.[52] Furthermore, compared to **^{S}P^{MeAN}**, which is unreactive toward phenols, the enhanced oxidative reactivity of **O^{MeAN}-LA** suggests that one important consequence of Lewis acid binding is to raise the reduction potential of the Cu_2O_2 core to allow heightened oxidative reactivity. Thus, Lewis acid coordination is a strategy that can not only effect the core structure (**^{S}P**/**O** equilibrium) but also may tune the reduction potential of the Cu_2O_2 core to facilitate substrate oxidation.

CONCLUSIONS

In this paper, we showed that the unreactive Cu_2O_2 core of **^{S}P^{MeAN}** could be activated by substrate binding (i.e., sodium 4-R-phenolates) and by Lewis acid addition triggering O–O cleavage to form **O^{MeAN}** cores. First, phenolate binding to the copper ion (primary coordination sphere) led to formation of a fleeting phenolate-bound dicopper(III) species (**O^{MeAN}-RPhO$^-$**) which was characterized by UV–vis and rR spectroscopies. TD-DFT calculations provided evidence that sequential phenolate binding as an axial ligand and isomerization to the equatorial form occurs before the r.d.s., where the **O** core electrophilically attacks the phenyl ring.

Second, we demonstrated that addition of Lewis acids to **^{S}P^{MeAN}** also led to O–O cleavage (**O^{MeAN}-LA** formation) with coordination of the different Lewis acids occurring at the secondary coordination sphere via binding to what was the axial N of the MeAN ligand. Importantly, the oxidative properties of the **O^{MeAN}-LA** species toward external substrates were influenced by the Lewis acid identity. Mechanistic studies provided evidence that C–H oxidation occurred via hydrogen atom transfer, with the borane adduct **O^{MeAN}-2BR$_3$** reacting slightly faster than did the **O^{MeAN}-2H$^+$** and **O^{MeAN}-Sc^{3+}** cores. Conversely, phenol oxidation was found to happen via stepwise electron-transfer proton-transfer (ET-PT), with

the $\mathbf{O^{MeAN}\text{-}2H^{+}}$ and $\mathbf{O^{MeAN}\text{-}Sc^{3+}}$ cores reacting much faster than the $\mathbf{O^{MeAN}\text{-}2BR_3}$ analogue.

These findings can inspire new routes to develop oxidation systems based on first row metals and dioxygen by utilizing Lewis acids to fine-tune the stereoelectronic properties of the reactive intermediates, leading potentially to novel selectivity patterns. Moreover, these results emphasize the importance of understanding the influence of the secondary as well as the primary coordination spheres in order to explain the speciation (type of Cu/O_2 species) and reactivity of metalloenzymes such as pMMO.

Supplementary Material

Refer to Web version on PubMed Central for supplementary material.

Acknowledgments

This research was supported by the U.S. NIH (GM60353 to K.D.K., DK31450 to E.I.S., and NRSA postdoctoral fellowship F32-GM105288 to R.E.C.). I.G.-B. thanks the Robert A. Welch Foundation for financial support (grant N-1900).

References

1. Solomon EI, Heppner DE, Johnston EM, Ginsbach JW, Cirera J, Qayyum M, Kieber-Emmons MT, Kjaergaard CH, Hadt RG, Tian L. Chem Rev. 2014; 114:3659. [PubMed: 24588098]
2. Solem E, Tuczek F, Decker H. Angew Chem, Int Ed. 2016; 55:2884.
3. Decker H, Schweikardt T, Tuczek F. Angew Chem, Int Ed. 2006; 45:4546.
4. Mirica LM, Vance M, Rudd DJ, Hedman B, Hodgson KO, Solomon EI, Stack TDP. Science. 2005; 308:1890. [PubMed: 15976297]
5. Citek C, Herres-Pawlis S, Stack TDP. Acc Chem Res. 2015; 48:2424. [PubMed: 26230113]
6. Rosenzweig AC. Nature. 2015; 518:309. [PubMed: 25607367]
7. Lawton TJ, Rosenzweig AC. J Am Chem Soc. 2016; 138:9327. [PubMed: 27366961]
8. Balasubramanian R, Rosenzweig A. Acc Chem Res. 2007; 40:573. [PubMed: 17444606]
9. Culpepper MA, Cutsail GE, Hoffman BM, Rosenzweig AC. J Am Chem Soc. 2012; 134:7640. [PubMed: 22540911]
10. Citek C, Lin BL, Phelps TE, Wasinger EC, Stack TDP. J Am Chem Soc. 2014; 136:14405. [PubMed: 25268334]
11. Yoshizawa K, Shiota Y. J Am Chem Soc. 2006; 128:9873. [PubMed: 16866545]
12. Mirica LM, Ottenwaelder X, Stack TDP. Chem Rev. 2004; 104:1013. [PubMed: 14871148]
13. Himes RA, Karlin KD. Curr Opin Chem Biol. 2009; 13:119. [PubMed: 19286415]
14. Lewis EA, Tolman WB. Chem Rev. 2004; 104:1047. [PubMed: 14871149]
15. Itoh S. Curr Opin Chem Biol. 2006; 10:115. [PubMed: 16504568]
16. Serrano-Plana J, Garcia-Bosch I, Company A, Costas M. Acc Chem Res. 2015; 48:2397. [PubMed: 26207342]
17. Halfen JA, Mahapatra S, Wilkinson EC, Kaderli S, Young VG Jr, Que L Jr, Zuberbühler AD, Tolman WB. Science. 1996; 271:1397. [PubMed: 8596910]
18. Kieber-Emmons MT, Ginsbach JW, Wick PK, Lucas HR, Helton ME, Lucchese B, Suzuki M, Zuberbühler AD, Karlin KD, Solomon EI. Angew Chem, Int Ed. 2014; 53:4935.
19. Kim S, Ginsbach JW, Billah AI, Siegler MA, Moore CD, Solomon EI, Karlin KD. J Am Chem Soc. 2014; 136:8063. [PubMed: 24854766]
20. Hatcher LQ, Karlin KD. JBIC, J Biol Inorg Chem. 2004; 9:669. [PubMed: 15311336]
21. Hatcher LQ, Karlin KD. Adv Inorg Chem. 2006; 58:131.

22. Park GY, Qayyum MF, Woertink J, Hodgson KO, Hedman B, Narducci Sarjeant AA, Solomon EI, Karlin KD. J Am Chem Soc. 2012; 134:8513. [PubMed: 22571744]
23. Company A, Palavicini S, Garcia-Bosch I, Mas-Balleste R, Que L, Rybak-Akimova EV, Casella L, Ribas X, Costas M. Chem - Eur J. 2008; 14:3535. [PubMed: 18348133]
24. Liang HC, Zhang CX, Henson MJ, Sommer RD, Hatwell KR, Kaderli S, Zuberbuehler AD, Rheingold AL, Solomon EI, Karlin KD. J Am Chem Soc. 2002; 124:4170. [PubMed: 11960420]
25. Garcia-Bosch I, Company A, Frisch JR, Torrent-Sucarrat M, Cardellach M, Gamba I, Gúell M, Casella L, Que L Jr, Ribas X, Luis JM, Costas M. Angew Chem, Int Ed. 2010; 49:2406.
26. Serrano-Plana J, Garcia-Bosch I, Miyake R, Costas M, Company A. Angew Chem, Int Ed. 2014; 53:9608.
27. Peterson RL, Himes RA, Kotani H, Suenobu T, Tian L, Siegler MA, Solomon EI, Fukuzumi S, Karlin KD. J Am Chem Soc. 2011; 133:1702. [PubMed: 21265534]
28. Frisch, MJ., Trucks, GW., Schlegel, HB., Scuseria, GE., Robb, MA., Cheeseman, JR., Scalmani, G., Barone, V., Mennucci, B., Petersson, GA., Nakatsuji, H., Caricato, M., Li, X., Hratchian, HP., Izmaylov, AF., Bloino, J., Zheng, G., Sonnenberg, JL., Hada, M., Ehara, M., Toyota, K., Fukuda, R., Hasegawa, J., Ishida, M., Nakajima, T., Honda, Y., Kitao, O., Nakai, H., Vreven, T., Montgomery, JA., Jr, Peralta, JE., Ogliaro, F., Bearpark, M., Heyd, JJ., Brothers, E., Kudin, KN., Staroverov, VN., Kobayashi, R., Normand, J., Raghavachari, K., Rendell, A., Burant, JC., Iyengar, SS., Tomasi, J., Cossi, M., Rega, N., Millam, JM., Klene, M., Knox, JE., Cross, JB., Bakken, V., Adamo, C., Jaramillo, J., Gomperts, R., Stratmann, RE., Yazyev, O., Austin, AJ., Cammi, R., Pomelli, C., Ochterski, JW., Martin, RL., Morokuma, K., Zakrzewski, VG., Voth, GA., Salvador, P., Dannenberg, JJ., Dapprich, S., Daniels, AD., Farkas, O., Foresman, JB., Ortiz, JV., Cioslowski, J., Fox, DJ. Gaussian 09 revision D.01. Gaussian Inc; Wallingford, CT: 2009.
29. Becke AD. J Chem Phys. 1993; 98:5648.
30. Lee C, Yang W, Parr RG. Phys Rev B: Condens Matter Mater Phys. 1988; 37:785.
31. Stephens PJ, Devlin FJ, Chabalowski CF, Frisch MJ. J Phys Chem. 1994; 98:11623.
32. Grimme S, Antony J, Ehrlich S, Krieg H. J Chem Phys. 2010; 132:154104. [PubMed: 20423165]
33. Yamaguchi K, Jensen F, Dorigo A, Houk KN. Chem Phys Lett. 1988; 149:537.
34. Gorelsky, SI. SWizard, version 4.2. University of Ottawa; Ottawa, Ontario, Canada: 2013. http://www.sg-chem.net/swizard/
35. Lee JY, Peterson RL, Ohkubo K, Garcia-Bosch I, Himes RA, Woertink J, Moore CD, Solomon EI, Fukuzumi S, Karlin KD. J Am Chem Soc. 2014; 136:9925. [PubMed: 24953129]
36. Matsumoto T, Ohkubo K, Honda K, Yazawa A, Furutachi H, Fujinami S, Fukuzumi S, Suzuki M. J Am Chem Soc. 2009; 131:9258. [PubMed: 19530656]
37. Op't Holt BT, Vance MA, Mirica LM, Heppner DE, Stack TDP, Solomon EI. J Am Chem Soc. 2009; 131:6421. [PubMed: 19368383] (b) The hydroxylation must occur through the equatorially-coordinated phenolate since the substrate ring must be attacked by the oxo in the Cu_2O_2 plane. Axial coordination of the phenolate places the substrate ring above the Cu_2O_2 plane; thus, the axial isomer must isomerize to the equatorial isomer to effect hydroxylation.
38. (a) Holland PL, Cramer CJ, Wilkinson EC, Mahapatra S, Rodgers KR, Itoh S, Taki M, Fukuzumi S, Que L, Tolman WB. J Am Chem Soc. 2000; 122:792.(b) Tang, J., Albrecht, AC. In Raman Spectroscopy. Szymanski, HA., editor. Vol. 2. Plenum; New York: 1970.
39. Chen J, Lee YM, Davis KM, Wu X, Seo MS, Cho KB, Yoon H, Park YJ, Fukuzumi S, Pushkar YN, Nam W. J Am Chem Soc. 2013; 135:6388. [PubMed: 23324100]
40. (a) Baglia RA, Dürr M, Ivanović-Burmazović I, Goldberg DP. Inorg Chem. 2014; 53:5893. [PubMed: 24873989] (b) Baglia RA, Krest CM, Yang T, Leeladee P, Goldberg DP. Inorg Chem. 2016; 55:10800. [PubMed: 27689821]
41. Yoon H, Lee YM, Wu X, Cho KB, Sarangi R, Nam W, Fukuzumi S. J Am Chem Soc. 2013; 135:9186. [PubMed: 23742163]
42. Park J, Lee YM, Nam W, Fukuzumi S. J Am Chem Soc. 2013; 135:5052. [PubMed: 23528016]
43. Henson MJ, Mukherjee P, Root DE, Stack TDP, Solomon EI. J Am Chem Soc. 1999; 121:10332.

44. The presence of this ~140 cm^{-1} mode was not directly observed due to significant elastic scattering of the Raman samples below 200 cm^{-1}. This mode has been directly observed along with its combination bands in a similar $Cu_2(\mu\text{-}O)_2$ complex; see ref 43.
45. (a) Several isomers of the **O^{MeAN}-LA** complexes were surveyed, including *cis*/*trans* and *syn*/*anti* orientation of the two uncoordinated ligand arms. The lowest energy structures are given in Figure 5. (b) An O-protonated **O^{MeAN}-$2H^+$** species was also evaluated computationally and was found to be energetically similar to the N-protonated species in Figure 5 (+0.5 kcal/mol); however, the calculated normal modes were inconsistent with the rR data (see Figure S25). Attempts to optimize **O^{MeAN}-$2BMe_3$** or **O^{MeAN}-$Sc(OTf)_2$** with O-bound Lewis acids invariably led to cleavage of a Cu–O bond and opening of the diamond core. Since these structures would not be consistent with the spectroscopy indicating bis(μ-oxo) cores, they were not evaluated further.
46. Leeladee P, Baglia RA, Prokop KA, Latifi R, de Visser SP, Goldberg DP. J Am Chem Soc. 2012; 134:10397. [PubMed: 22667991]
47. Li F, Van Heuvelen KM, Meier KK, Münck E, Que L. J Am Chem Soc. 2013; 135:10198. [PubMed: 23802702]
48. Bang S, Lee YM, Hong S, Cho KB, Nishida Y, Seo MS, Sarangi R, Fukuzumi S, Nam W. Nat Chem. 2014; 6:934. [PubMed: 25242490]
49. Osako T, Ohkubo K, Taki M, Tachi Y, Fukuzumi S, Itoh S. J Am Chem Soc. 2003; 125:11027. [PubMed: 12952484]
50. A linear relationship was also found between the reaction rates and the BDFE of the phenols (only three values available), with the BDFE directly proportional to E^0 and the pK_a.
51. Garcia-Bosch I, Ribas X, Costas M. Chem - Eur J. 2012; 18:2113. [PubMed: 22250002]
52. Dhar D, Yee GM, Markle TF, Mayer JM, Tolman WB. Chem Sci. 2017; 8:1075. [PubMed: 28572905]

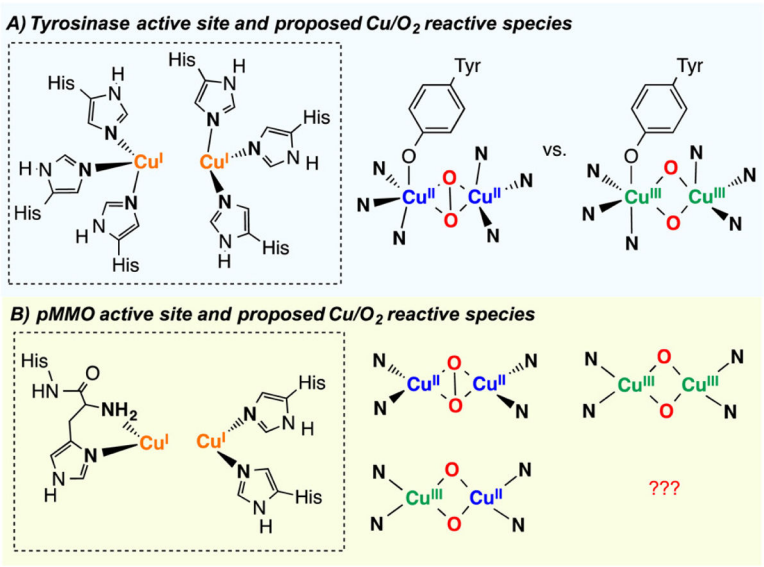

Figure 1.

Active site and proposed Cu/O_2 reactive species of (A) tyrosinase (Ty) and (B) particulate methane monooxygenase (pMMO).

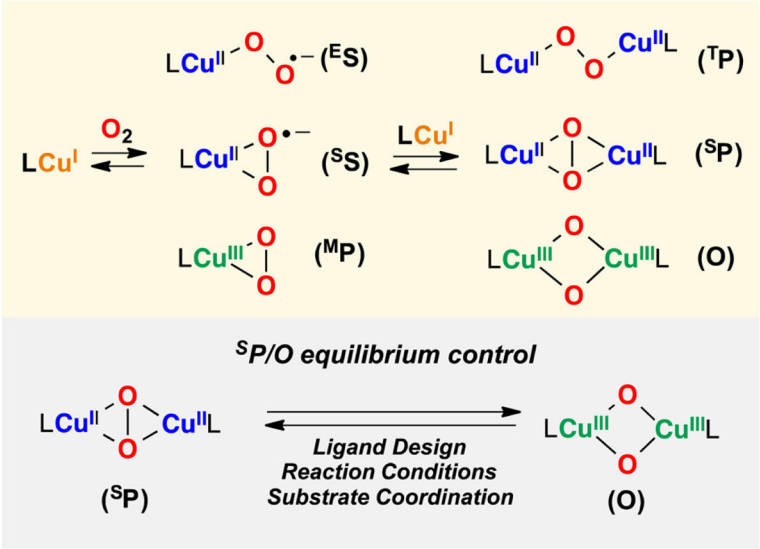

Figure 2.

Top: Common LCu/O_2 species derived from the oxygenation of copper(I) complexes. Bottom: Control of the ^{S}**P**/**O** equilibrium by different means.

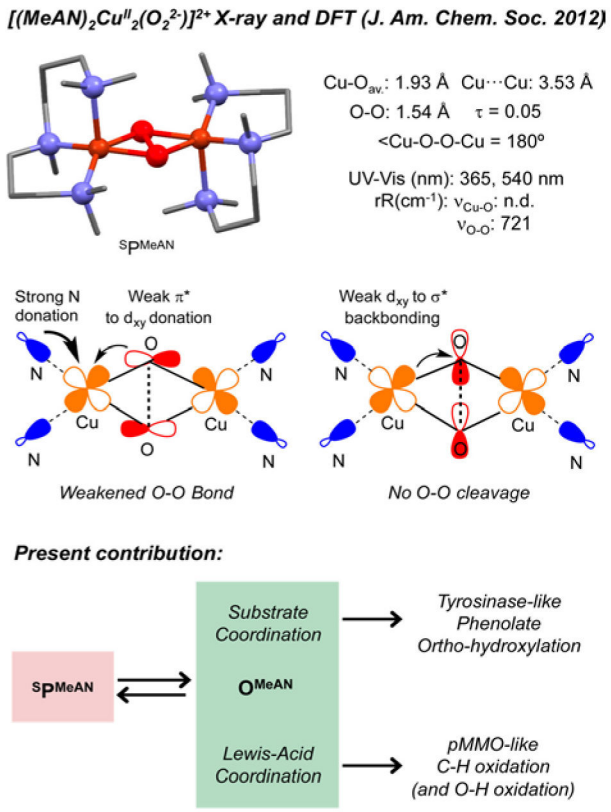

Figure 3.

Top: **^{S}P^{MeAN}** X-ray structure and its geometric and spectroscopic features. Middle: Molecular orbital diagrams of the **^{S}P^{MeAN}** core that lead to lengthening of the O–O bond without concomitant O–O cleavage. Bottom: Subjects of this report: coordination of phenolates and Lewis acids to **^{S}P^{MeAN}** imparts tyrosinase-like hydroxylation and pMMO-like C–H oxidation reactivity through **O^{MeAN}**.

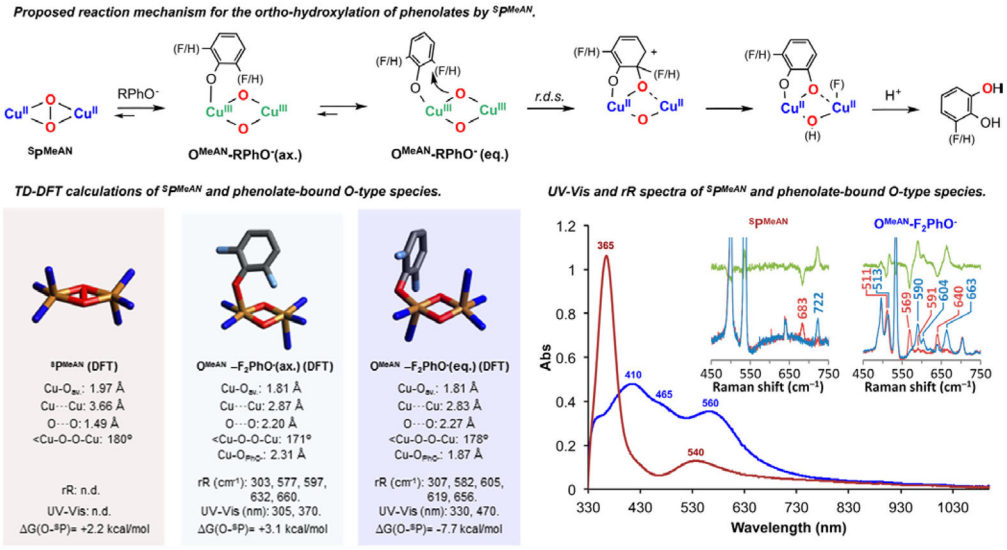

Figure 4.

Top: Postulated reaction mechanism of **^{S}P^{MeAN}** toward sodium phenolates to generate the corresponding *ortho*-hydroxylated products through **O^{MeAN}-RPhO^{-}**. Bottom left: Core structures of DFT-optimized **^{S}P^{MeAN}** and **O^{MeAN}-RPhO^{-}** with relevant metrical parameters, calculated Cu–O normal modes, TD-DFT-calculated LMCT energies, and energy of peroxo isomers relative to the corresponding bis(μ-oxo) isomers. Bottom right: Absorption spectra of **^{S}P^{MeAN}** (brown) and intermediate **O^{MeAN-}F$_2$PhO^{-}** (blue). Inset: Resonance Raman spectra of **^{S}P^{MeAN}** (λ = 413.1 nm) and **O^{MeAN-}F$_2$PhO^{-}** (λ = 568.2 nm) with $^{16}O_2$ (blue), $^{18}O_2$ (brown), and the $^{16}O_2$-$^{18}O_2$ difference spectra (green).

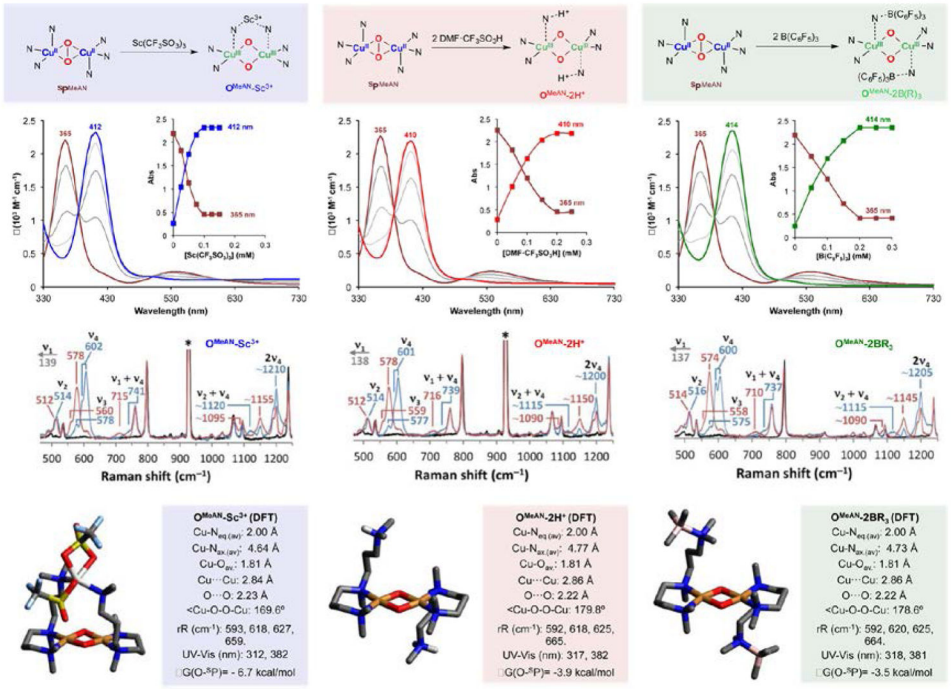

Figure 5.

Top: Generation of the different **O^{MeAN}-LA** complexes. Middle: Spectroscopic characterization of the **O^{MeAN}-LA** series by UV–vis (inset shows titration experiments) and rR at 413.1 nm excitation ($^{16}O_2$ in blue, $^{18}O_2$ in red, and Cu(I) background in black). Mode assignments are indicated, and instrument artifacts are marked with (*). Bottom: Structures of DFT-optimized **O^{MeAN}-LA species** with relevant metrical parameters, calculated Cu–O normal modes, TD-DFT-calculated LMCT energies, and energy of peroxo isomers relative to the corresponding bis(μ-oxo) isomers.

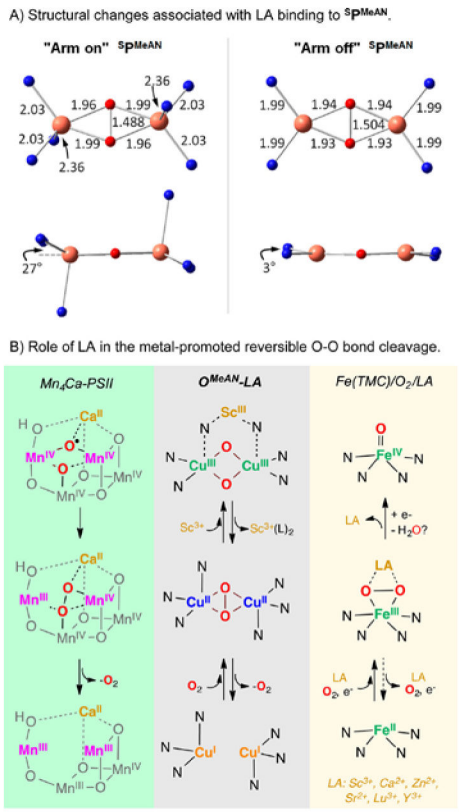

Figure 6.

(A) DFT-optimized structures of $^{S}\mathbf{P}^{\mathbf{MeAN}}$ with the axial amine ligand arm in an (left) “on” binding position as observed experimentally by crystallography, and (right) “off” binding position. Top: core geometry and bond lengths (Å). Bottom: core structure viewed perpendicular to the Cu_2O_2 plane, showing the smaller deviation of the equatorial N ligands out of the Cu_2O_2 plane in the “arm off” isomer. (B) Role of Lewis acids in O–O bond formation at the active center of Photosystem II (left), the reversible O–O cleavage shown in the $^{S}\mathbf{P}^{\mathbf{MeAN}}/\mathbf{O}^{\mathbf{MeAN}-}$ **LA** series (middle) and O–O cleavage in nonheme iron(III)-peroxo reduction/oxidation (right).

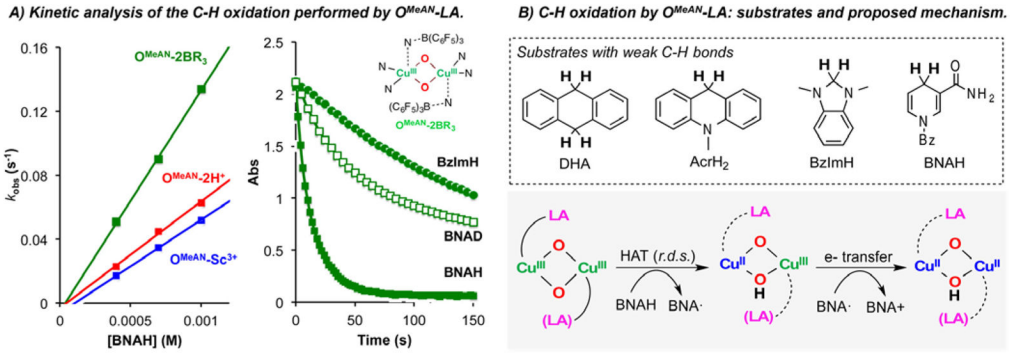

Figure 7.

C–H oxidations performed by **O^{MeAN}-LA** cores: (A) kinetic analysis of the reaction (see Supporting Information for further details); (B) substrates used and proposed mechanism for HAT + e^- transfer.

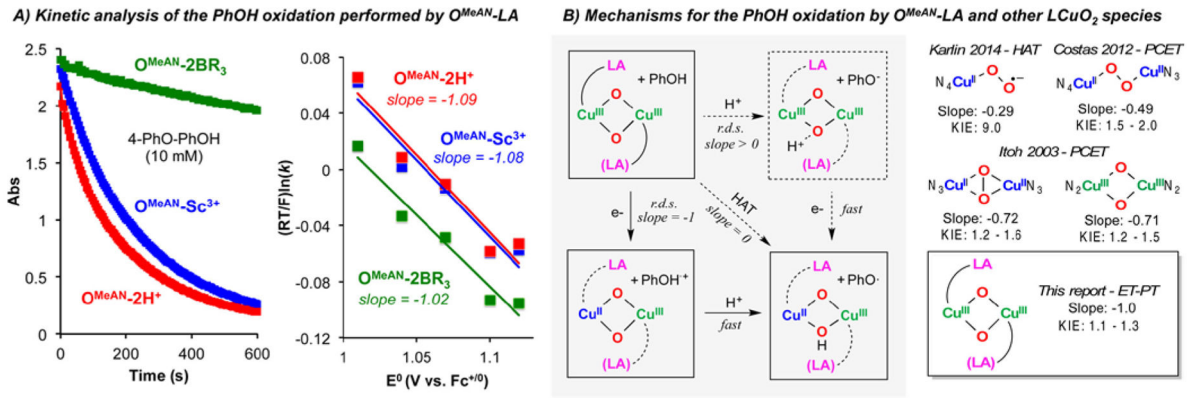

Figure 8.

O–H oxidation performed by **O^{MeAN}-LA** cores: (A) kinetic analysis; (B) possible reaction mechanisms and comparison of KIEs (see Figure S18) and reduction potential effects to literature examples.

Table 1

Kinetic Parameters of C–H Oxidation Reactions by O^{MeAN}-LA

substrate	BDE ($H^{\bullet}$) (kcal/mol)	BDE (H^{-}) (kcal/mol)	$k^{OMeAN32H+}$ (M^{-1} s^{-1})	$k^{OMeAN3Sc3+}$ (M^{-1} s^{-1})	$k^{OMeAN32BR3}$ (M^{-1} s^{-1})	notes
BNAH	70.7	64.2	66 ± 1	58 ± 1	138 ± 2	yield: 80–99%
BNAD			7.8 ± 0.1 (KIE: 8.5)	5.7 ± 0.1 (KIE: 10.3)	22.7 ± 0.3 (KIE: 6.1)	
BzImH	73.4	49.5	12.1 ± 0.2[a]	6.0 ± 0.1[b]	19.1 ± 0.2[c]	$k^{BNAH/BzImH}$: 5.5, 9.7, 7.2[a,b,c]
$AcrH_2$	73.0	81.1	too slow	too slow	too slow	less than 5% decay after 1 h
DHA	76		no reaction	no reaction	no reaction	no decay (t = 1 h, −90 °C)

[a] $k_{OMeAN-2H+}$.

[b] $k_{OMeAN-Sc3+}$.

[c] $k_{OMeAN-2BR3}$.

Table 2

Kinetic Parameters of O–H Oxidation Reactions by O^{MeAN}-LA

substrate	BDE (H•) (kcal/mol)	E^0 (V vs $Fc^{+/0}$)	$k^{OMeAN32H+}$ (M^{-1} s^{-1})	$k^{OMeAN3Sc3+}$ (M^{-1} s^{-1})	$k^{OMeAN32BR3}$ (M^{-1} s^{-1})	notes
4-MeO-PhOH	80.9	1.01	64 ± 1	53 ± 1	2.9 ± 0.2	*a*
4-MeO-PhOD		1.01	52 ± 1 (KIE: 1.25)	42 ± 1 (KIE: 1.19)	2.4 ± 0.1 (KIE: 1.17)	*a*
2,4-$^tBu_2$-PhOH	81.9	1.04	1.8 ± 0.2	1.1 ± 0.1	0.12 ± 0.01	yield: 60–70%
4-PhO-PhOH		1.07	0.51 ± 0.02	0.44 ± 0.02	0.046 ± 0.001	*a*
4-^{t}Bu-PhOH		1.10	0.025 ± 0.001	0.023 ± 0.001	0.0027 ± 0.0003	*a*
4-Me-PhOH	84.6	1.12	0.035 ± 0.002	0.027 ± 0.001	0.0024 ± 0.0002	*a*
4-Cl-PhOH	85.7	1.21	no reaction	no reaction	no reaction	no decay (t = 1 h)

[a]Product not quantified (see text and Supporting Information).